J. Fluid Mech. (1996), vol. 320, pp. 259–285

Very large structures in plane turbulent Couette flow

By JUKKA KOMMINAHO[1], ANDERS LUNDBLADH[2]† AND ARNE V. JOHANSSON[1]

[1]Royal Institute of Technology, Department of Mechanics, Stockholm, Sweden

[2]FFA, Bromma, Sweden

(Received 1 June 1995 and in revised form 26 March 1996)

A direct numerical simulation was carried out of plane turbulent Couette flow at a Reynolds number of 750, based on half the velocity difference between the walls and half the channel width. Particular attention was paid to choosing a computational box that is large enough to accommodate even the largest scales of the turbulence. In the central region of the channel very large elongated structures were observed, in accordance with earlier findings. The study is focused on the properties of these structures, but is also aimed at obtaining accurate turbulence statistics. Terms in the energy budget were evaluated and discussed. Also, the limiting values of various quantities were determined and their relevance in high Reynolds number flows discussed. The large structures were shown to be very sensitive to an imposed system rotation. They could be essentially eliminated with a stabilizing system rotation (around the spanwise axis) small enough for only minor damping of the rest of the scales. Despite the fact that the large structures dominate the appearance of the flow field their energy content was shown to be relatively small, on the order of 10% of the total turbulent kinetic energy.

1. Introduction

Plane Couette flow, i.e. flow between two plane infinitely large parallel planes, is one of the canonical flow cases. A fully developed plane Couette flow has a constant shear stress across the entire channel. It also has a monotonic velocity profile (see figure 1), laminar or turbulent. The existence of a non-zero mean shear rate, and associated turbulence production at the centre of the channel, gives a significantly different character to the flow in this region, as compared to pressure-driven channel flow.

In comparison with zero-pressure-gradient boundary layers and pressure-driven channel flow, plane Couette flow has the unique feature of combining the parallel flow property with a zero pressure gradient. This suggests that one would expect similarities with boundary layer flow, but with a significantly simpler mean flow equation.

Numerical simulation of fully developed channel flow has successfully been carried out in a number of studies (see e.g. Kim, Moin & Moser 1987), but plane Couette flow has proven to be more difficult to simulate numerically. Plane Couette flow is also difficult to establish experimentally, and experiments are hence scarce although recently several reports on plane Couette flow have appeared.

† Present address: Volvo Aero Corp. 461 81 Trollhättan, Sweden.

One approach to obtain Couette flow in experiments is to have one stationary and one moving wall. This setup is suitable for hot-wire anemometry since the disturbances introduced by the probe will propagate out from the channel.

Another approach taken is to have an apparatus with counter-moving walls. The fully developed state is reached through diffusion of vorticity from the walls across the channel. Such an apparatus is suitable for non-intrusive measurements such as LDV. Probes inserted in this setup will give rise to disturbances that propagate in both directions, since there is no net transport of fluid.

The earliest reported experiments on plane Couette flow are those of Reichardt (1956) in a running belt apparatus with both belts moving. In this study he used oil and water as fluids, and reported measurements of mean velocity profiles. He also later reported measurements from an air-flow apparatus with one moving wall with a fan at the inlet to obtain the correct mass flux through the channel (Reichardt 1959). He observed the characteristic S-shape of the mean turbulent velocity profile at various Reynolds numbers up to 17000, based on half the velocity difference between the walls and half the channel width.

Reichardt also tried to determine the transitional Reynolds number, i.e. the lowest Reynolds number for which turbulence is sustained. He arrived at a value of 750. A number of different results for the transitional Reynolds number were later reported, but it is now well established, both from direct numerical simulations and experiments, that this value is close to 360 (see Lundbladh & Johansson 1991; Tillmark & Alfredsson 1992; Komminaho, Lundbladh & Johansson 1995).

Robertson & Johnson (1970) made measurements in air in a belt-type apparatus with one wall moving (with a fan at the inlet), and reported measurements of mean velocity and turbulence data such as two-point correlations and streamwise turbulence intensity. More recent experiments are those of El Telbany & Reynolds (1982), who used a moving belt and one rigid wall, again together with an inlet blower to establish the flow. The Reynolds number ranges covered in these studies are 7000–16500 and 9500–19000, respectively. It is clear from these measurements that the turbulence intensities in the central region are substantially higher than in pressure-driven turbulent channel flow. In particular, the streamwise intensity is almost twice as high as in channel flow. From these and Reichardt's experiments it is also clear that the normalized mean shear at the centre remains practically constant (or decreases very slowly) with increasing Reynolds number. This gives a non-zero turbulence production in the central region, which explains the higher turbulence levels there.

An extensive set of experiments on turbulent and transitional plane Couette flow has recently been carried out by Tillmark and co-workers (see e.g. Tillmark & Alfredsson 1992; Bech *et al.*1995; Tillmark 1995). The apparatus used in these experiments allowed both one- and two-moving-wall setups. Hot-wire anemometry and LDV were used to determine various one-point turbulence statistics, as well as two-point correlations and turbulence structure.

For further references on experimental investigations of plane Couette flow and a discussion of these, the reader is referred to Tillmark (1995).

The first direct numerical simulation of fully developed turbulent plane Couette flow was carried out by Lee & Kim (1991) who observed very long structures with a roughly circular cross-section, extending through the channel. These give a structure of the turbulence in the central region that is quite different than in channel flow. They used a pseudo-spectral method with $128 \times 129 \times 192$ spectral modes and a computational box of $4\pi \times 2 \times 8\pi/3$, at a Reynolds number of 3000. They chose the spanwise extent of their computational domain so as to contain two pairs of the large structures,

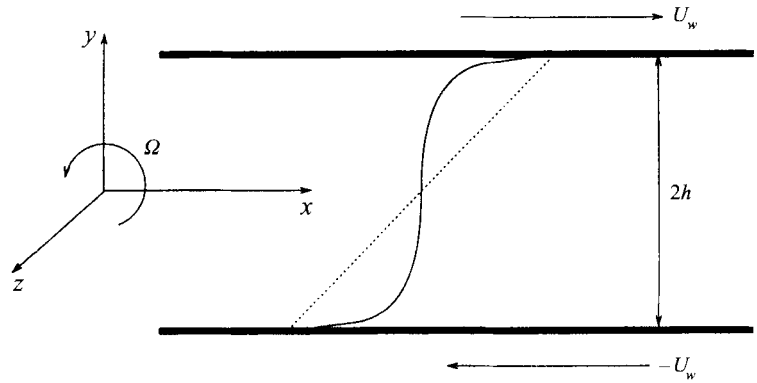

FIGURE 1. The flow geometry in plane Couette flow: —, turbulent mean velocity profile; · · ·, laminar mean velocity profile.

which may have caused an artificial forcing of these. In their computations they found these large structures to extend all the way through the box (in the streamwise direction), and to be almost uniform in the streamwise direction. They also report that these structures contribute about 30% of the turbulent kinetic energy. When they extended the box to more than $1000h$ the structures persisted, although these results are from simulations with very low resolution and are therefore of doubtful value.

Kristoffersen, Bech & Andersson (1993) used a code based on finite differences, second-order central space, with a staggered grid arrangement. The computational domain was $4\pi \times 2 \times 2\pi$, and the number of grid points $96 \times 64 \times 64$, at a Reynolds number of 1300. They found fairly high values of the two-point velocity correlations for the streamwise velocity for the maximum streamwise separation, which indicates that the computational box is too short. They also found large structures to extend throughout the box.

In a later study with the same code (Bech *et al.* 1995) they used a larger box ($10\pi \times 2 \times 4\pi$) and $256 \times 70 \times 256$ grid points at a Reynolds number of 1300. These results were reported together with experimental data. As we shall see from the present study also this box is probably too short to accommodate the largest scales.

A related direct numerical simulation study by Papavassiliou & Hanratty (1996) was brought to our attention by one of the referees. Unfortunately this paper was still unavailable for comparison at the time of this writing.

The present study is aimed at investigating the large-scale structures in plane Couette flow turbulence, as well as giving accurate turbulent statistics. Investigations of the effect of limited box size on the large scales and on the turbulence intensities are carried out. We will compare our results with experimental data, and in particular with those of Bech *et al.*, (1995, referred to herein as BTAA). Also, the effect of a slow system rotation around the spanwise axis is investigated. The effect on the large structures and on the turbulence statistics is reported. Since no experiments of this flow case exists today, comparison with measured data is not possible.

2. Numerical requirements

The simulation code used for the present computations uses spectral methods to solve the Navier–Stokes equations, with Fourier representation in the streamwise (x) and spanwise (z) directions, and Chebyshev polynomials in the wall-normal (y)

Case	Computational domain	Number of modes	Resolution	Time	T_{stat} rate	Rotation
1	$8 \times 2 \times 4$	$32 \times 55 \times 32$	$13 \times 1.9 \times 6.5$	4000	3500	-
2a	$10\pi \times 2 \times 4\pi$	$85 \times 33 \times 42$	$19 \times 3.2 \times 15.6$	200	-	-
2b	$10\pi \times 2 \times 4\pi$	$120 \times 55 \times 85$	$13.6 \times 1.9 \times 7.7$	1150	1050	-
3a	$28\pi \times 2 \times 8\pi$	$85 \times 33 \times 42$	$54 \times 3.2 \times 31$	200	-	-
3b	$28\pi \times 2 \times 8\pi$	$170 \times 49 \times 85$	$27 \times 2.1 \times 15.4$	900	-	-
3c	$28\pi \times 2 \times 8\pi$	$340 \times 55 \times 170$	$13.5 \times 1.9 \times 7.7$	920	620	-
4a	$28\pi \times 2 \times 8\pi$	$340 \times 55 \times 170$	$13.5 \times 1.9 \times 7.7$	280	150	-0.005
4b	$28\pi \times 2 \times 8\pi$	$340 \times 55 \times 170$	$13.5 \times 1.9 \times 7.7$	600	200	-0.015
4c	$28\pi \times 2 \times 8\pi$	$340 \times 55 \times 170$	$13.5 \times 1.9 \times 7.7$	100	-	-0.03

TABLE 1. Parameters for the various simulation cases. The computational domain is measured in half-channel heights, and the resolution is scaled in wall units. The resolution given for the wall-normal direction is the mean spacing. T_{stat} denotes the time over which the statistics were averaged. All quantities in the table are in the streamwise, wall-normal and spanwise directions, respectively.

direction. The nonlinear terms are treated pseudo-spectrally using FFTs. The program was originally written in Fortran 77 to run on vector machines, but has been ported to run on a massively parallel machine, the Thinking Machines CM-200. Aliasing errors from the evaluation of the nonlinear term were removed by the $\frac{2}{3}$-rule. The time-stepping scheme used is semi-implicit, with a third-order Runge–Kutta method for the nonlinear term and a second-order Crank–Nicolson method for the linear term. The time step was dynamically kept at 90% of the theoretical CFL limit. Periodic boundary conditions were used in x- and z-directions, with the no-slip condition at the walls.

The flow situation is sketched in figure 1. If not otherwise stated all quantities are normalized by U_w and h, denoting the wall velocity and half the separation between the infinitely large plates that drive the flow. Non-dimensionalization with wall variables is used when appropriate and denoted by plus superscript, e.g. $y^+ = yu_\tau/\nu$ where $u_\tau = (\tau_w/\rho)^{1/2}$ is the friction velocity.

We have carried out simulations with three different sizes of the computational domain. For the smallest domain the simulation was directly started with a high resolution. For the two larger domains the simulations were started with a coarse resolution that was refined when the flow had reached a statistical steady state. The final resolution was equal in all three simulations, and comparable to that in the turbulent channel flow simulation by Kim *et al.* (1987, hereinafter referred to as KMM). The initial conditions were chosen as a set of random modes without any symmetries. To avoid effects of the transients caused by the change of resolution the first few hundred time units from the simulations with the final resolution were discarded in the evaluation of the flow statistics. For more details concerning the simulations see table 1.

The computations totalled more than 550 CPU hours on a CM-200 with 8k processors. The performance of the code for the largest problem size was about 240 Mflops, and the memory requirements about 900 Mbyte.

The resolution must be high enough to resolve all relevant scales of the flow. For the largest box and the finest resolution the two-dimensional energy spectrum, $\Phi(k_x, k_z)$, obtained by integrating the corresponding three-dimensional spectrum in the y-direction is shown in figure 2. The general structure of the energy spectrum is

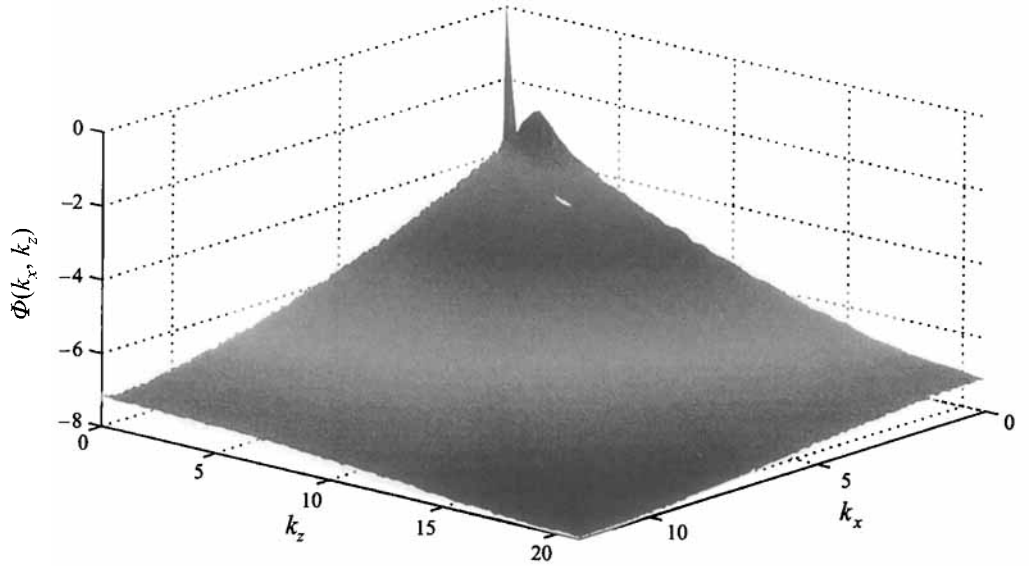

FIGURE 2. The logarithm of the two-dimensional energy spectrum $\Phi(k_x, k_z)$, normalized with $\max \Phi(k_x, k_z)$, as function of streamwise (k_x) and spanwise (k_z) wavenumbers.

somewhat different from that in channel flow, and the peak at $k_z \approx 1.5/h$ is associated with the large structures that we will discuss in detail later. The peak is quite sharp, signified by the fact that the energy density is larger than half the peak value in as small a range of streamwise wavenumber as 0–$0.21/h$. To estimate the 'excess' energy content in the peak the spectrum was compared with one for a case with stabilizing spanwise rotation where the large structures are essentially completely eliminated (see §4). From this comparison we conclude that the excess energy in the peak in figure 2 is roughly 10% of the total fluctuation energy. The wavenumbers included for this comparison are those with an energy density larger than half the peak value.

There is no sign of energy build-up at high wavenumbers. Also the energy density distribution over the Chebyshev modes obtained by integrating in the x- and z-directions, falls a total of seven decades from its maximum value. A similar trend is also seen for $\Phi(k_x, k_z)$ in figure 2. Altogether this indicates that the resolution used is sufficient in all three directions.

The use of three different sizes of the computational domain enables us to investigate the effects of too small a box and to ensure that the results in the largest simulation are converged to those of an infinite domain with a good accuracy. If the box is smaller than the largest eddies these will artificially become infinitely long due to the periodic boundary conditions. They will couple over the box to enhance those that are aligned in the streamwise direction, and conversely inhibit the large structures that have a non-zero angle with respect to the mean flow direction. From inspection of the simulated data, we could observe that the large eddies tend to be highly elongated and that the deviation from alignment in the streamwise direction typically is small. In the smaller boxes this tendency is quite exaggerated and the largest eddies will be artificially amplified (by the periodic boundary condition) causing an overprediction of the two-point velocity correlations for large separations. We will here examine in some detail the influence of the box length on the two-point streamwise velocity correlation with streamwise and spanwise separation. Also the influence on the time-averaged velocity r.m.s. values is studied.

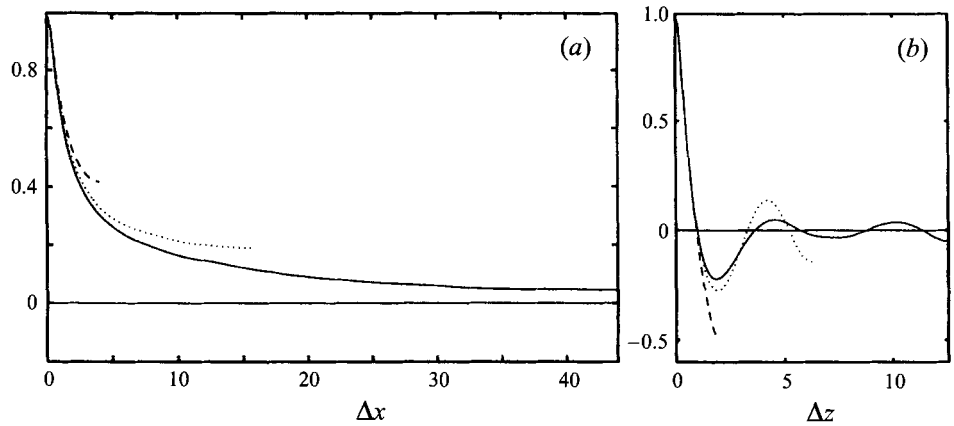

FIGURE 3. The two-point correlation for the streamwise velocity R_{uu} at $y = 0$ for different box sizes: $28\pi \times 2 \times 8\pi$ (—), $10\pi \times 2 \times 4\pi$ (···), and $8 \times 2 \times 4$ (— —) (*a*) for streamwise separation, (*b*) for spanwise separation.

In figure 3 we show two-point velocity correlation curves for the streamwise velocity at $y = 0$, for the three different box sizes. A further effect that tends to give an overpredicted value of the correlation $R_{uu}(\Delta x)$ at half the box length is the symmetry properties of R_{uu} that cause the derivative to be zero at the maximum separation. This means that the two-point correlation for the streamwise velocity $R_{uu}(\Delta x)$ is always overpredicted at half the box length. The situation is therefore somewhat better than what would be judged from figure 3(*a*). It can be concluded though from figure 3(*a*) that this flow case requires a very long box, much longer than is needed for the simulation of turbulent channel flow. Closer to the wall the correlation is lower, and the integral length scales are smaller. This is in contrast to channel flow where the integral length scales are larger closer to the wall. In the $8 \times 2 \times 4$ box the correlation $R_{uu}(\Delta z)$ in figure 3(*b*) is strongly negative at a spanwise separation of half the box width. The box is here only 4 half-channel heights wide, leaving room for only one pair of the large structures. This pair couples strongly over the box, causing the correlation with streamwise separation to also become much higher than for an infinite box. For the largest box this effect is virtually eliminated since there is room for a number of such pairs. The periodic boundary condition is adequate here. One should note that a very wide box is required to obtain small correlations. For spanwise separations the correlation is also overpredicted at half the box width due to the symmetry property of the correlation function.

The time- and (x,z)-plane-averaged u_{rms} values (figure 4) for the smallest box are considerably higher than for the other two, indicating that this box is totally inadequate for obtaining accurate quantitative data for Couette flow. The reason for the artificially high energy content in the large scales has been discussed above. The u_{rms} values for the largest box have converged to the value for an infinite box. The discrepancy with an infinitely large box can be judged to be less than 1% in u_{rms}. Note that it is of great interest to achieve this kind of accuracy in order to be able to detect even small Reynolds number dependencies. We may here mention the weak Reynolds number trend for $(u_{rms})_{max}$ observed in channel flow simulations (see Antonia & Kim 1994). The maximum of u_{rms}/u_τ was found to increase from 2.67 to 2.74 for roughly a threefold increase in Reynolds number. The differences in the v_{rms} and w_{rms} values for different box sizes are smaller than for u_{rms}.

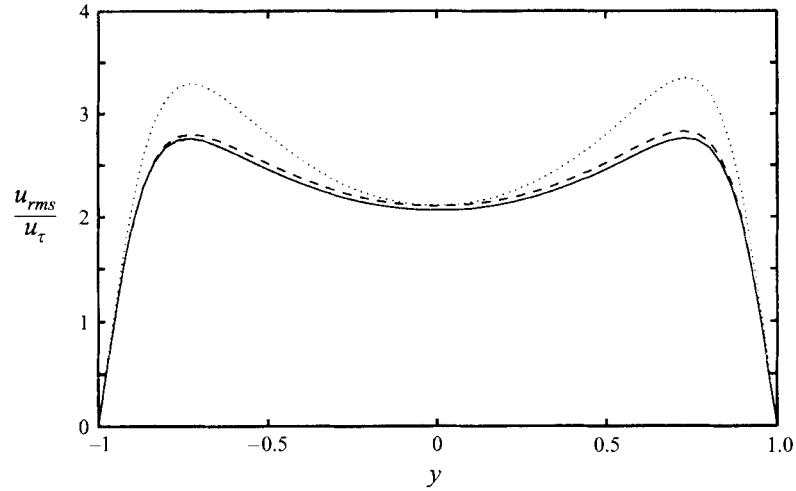

FIGURE 4. The u_{rms}/u_τ values for the different box sizes as a function of y: $28\pi \times 2 \times 8\pi$ (—), $10\pi \times 2 \times 4\pi$ (— —), and $8 \times 2 \times 4$ (· · ·).

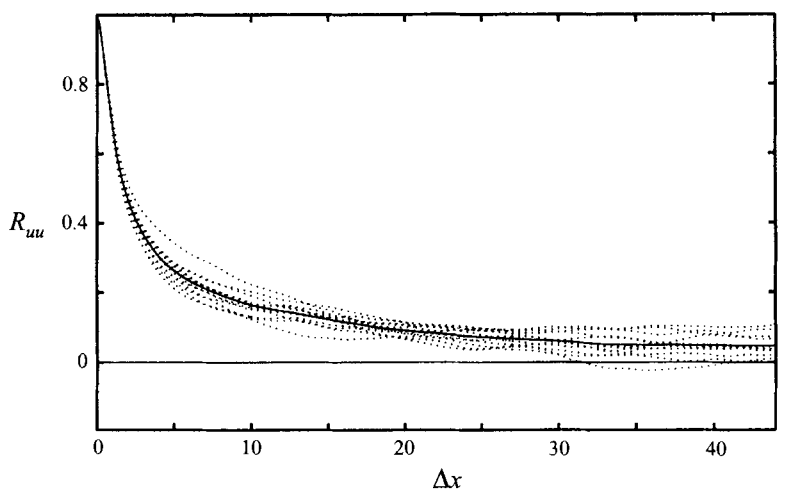

FIGURE 5. $R_{uu}(\Delta x)$ at $y = 0$, averaged over 600 time units (—), different realizations averaged over 50 time units (· · ·).

Another important aspect of the simulations is the requirement for the length of the time interval needed for the averaging of the flow statistics. The time scales for integral quantities are longer than for instantaneous ones, and we will therefore take a closer look at the averaging of $R_{uu}(\Delta x)$ and the integral length scale (Λ_{uux}) at $y = 0$.

We can see in figure 5 that the short time averages of $R_{uu}(\Delta x)$, averaged over 50 time units, fluctuate considerably even for rather small separations. Hence, in order to determine the correlation curve and integral length scales accurately there is a need to take the simulation to very large times. A running time average over $R_{uu}(L_{box}/2)$ has converged to 0.05 at the final time, with an error of less than ± 0.02. As pointed out earlier, though, this is an overprediction of the real correlation because of the symmetry properties of the correlation curve.

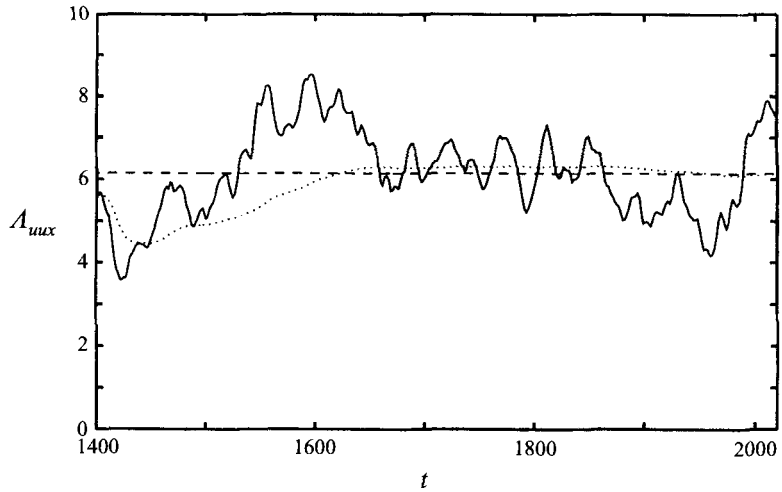

FIGURE 6. $\Lambda_{uux}(t)$ at $y = 0$: —, instantaneous value; · · ·, running time average; – –, final time averaged value.

The running time average of the streamwise integral length scale, Λ_{uux}, is shown in figure 6 and it has converged to 6.1 at the final time, with an estimated error of less than ± 0.3. The error is estimated by studying the maximum and the minimum of the last half of the running-time-average curve, i.e. the last 310 time units of the dotted line in figure 6.

With the above tests we may safely consider the resolution used to be adequate, the box size used to be sufficiently large, and the integration time to be sufficient to give good statistics, and good integral quantities. In the next section we will examine the statistical properties of the flow in the largest box.

3. Plane turbulent Couette flow

The flow situation and general character of the mean velocity profile are sketched in figure 1 for turbulent plane Couette flow. The Reynolds number based on half-channel height and half the velocity difference between the walls is 750 in all simulations discussed here. The Reynolds number

$$Re_\tau = \frac{hu_\tau}{\nu} = \left(\frac{h^2}{\nu} \frac{\mathrm{d}U}{\mathrm{d}y}\bigg|_w \right)^{1/2}$$

is 52.0. This is approximately a factor two higher than the lowest Reynolds number for which turbulence is sustained (Komminaho *et al.* 1995; Lundbladh & Johansson 1991; Tillmark & Alfredsson 1992).

In figure 7, the instantaneous streamwise velocity field in an (x,z)-plane at $y = 0$ is shown in the form of a grey-scale coding of the velocity. We can clearly see the large elongated structures aligned in the streamwise direction in the form of alternatingly high- and low-speed streaks. Note that the box is as large as 88×25 in the horizontal plane, or about 42 times larger in area than the box used in the channel flow simulation of KMM.

The large structures give large correlations for large separations mainly for the streamwise component, illustrating the fact that they mainly have a streak nature

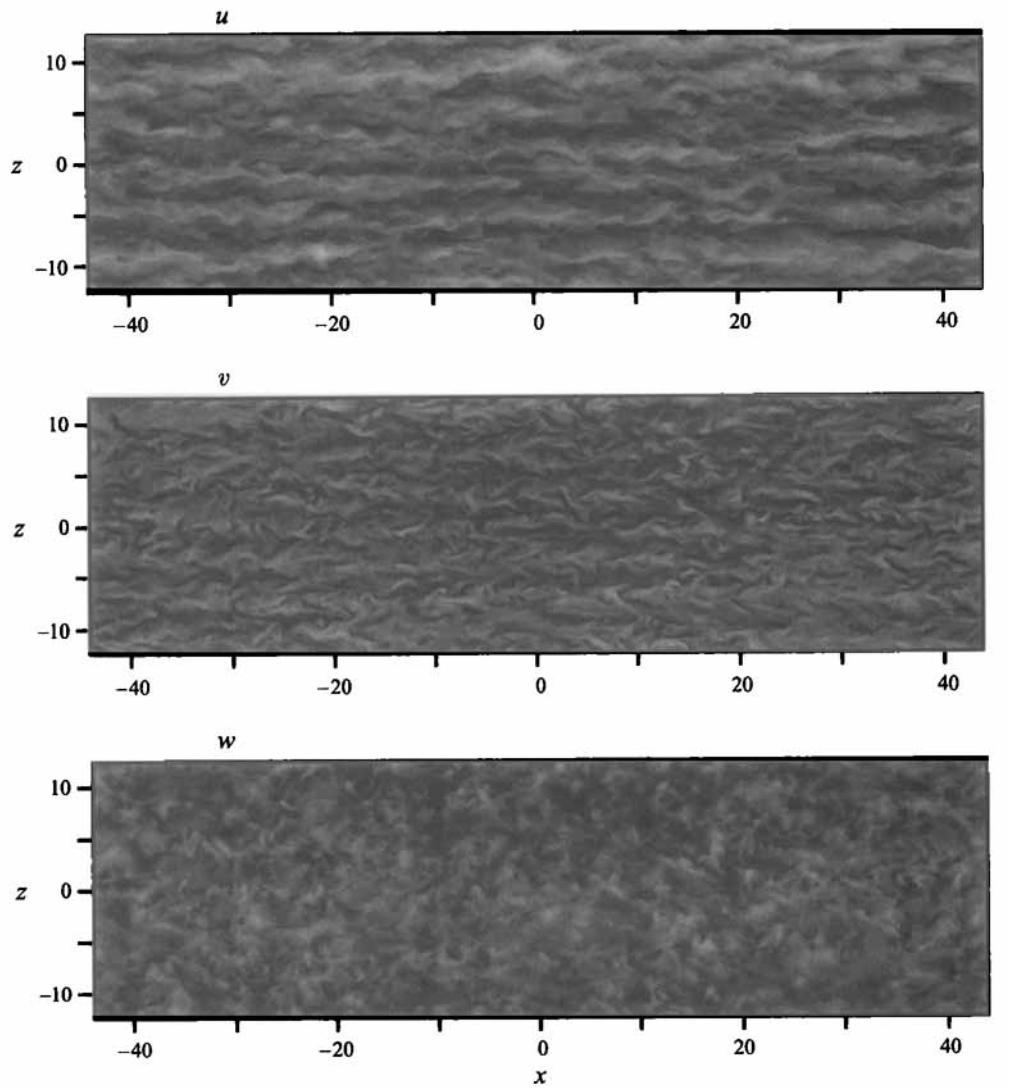

FIGURE 7. Instantaneous velocity fields at $T = 2020$ in an (x, z)-plane at $y = 0$. Streamwise velocity range -0.5 to 0.5; wall normal velocity range -0.3 to 0.3; spanwise velocity range -0.4 to 0.4.

with a weak associated streamwise vorticity. The large scales in u compared to the other velocity components are obvious from figure 7.

A cross-sectional view of the large structures is shown for two different times in figure 8(*a,b*). Here the small streamwise scales are filtered out by simply averaging the instantaneous fluctuating field over the x-direction. Velocity vectors in the (y,z)-plane are shown with superimposed contours of the streamwise fluctuating velocity. One can clearly observe distinct vortex patterns that fill the entire gap between the plates and are roughly circular in cross-section.

These vortex patterns have also been observed by Lee & Kim (1991) but whereas they found them to be essentially both fixed in position and stationary in time, our simulations show that in a sufficiently large box neither of these holds. In figure 8(*b*) we can see several distinct pairs of the vortex structures for $z < 0$, whereas the

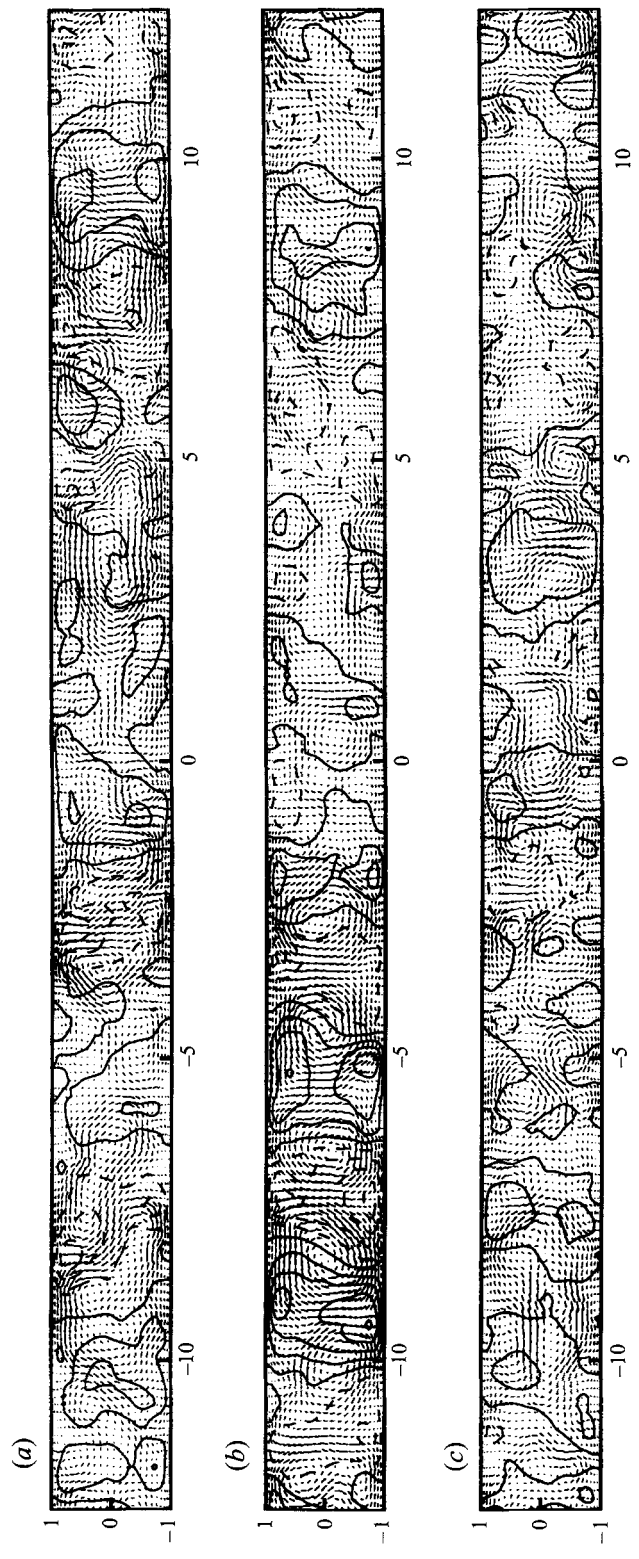

FIGURE 8. Velocity field, averaged over the x-axis, viewed in a (y,z)-plane, for different times. The solid contours denote $u \geqslant 0$, and dashed contours denote $u < 0$. The contour increment is 0.05. The v and w velocities are superimposed as vectors. For clarity every second point in the y-direction has been omitted. (*a*) $T = 1820$, (*b*) $T = 2020$, (*c*) $T = 2300$, $\Omega = -0.005$.

pattern is less distinct for $z > 0$. Also, in figure 8(*a*), we see a few distinct pairs of these structures, but now at z-values between 2 and 10. The streaks are thus neither stationary in time nor fixed in position. One further thing may be noted: when the integral length scale, Λ_{uux}, is high the vortex pattern is more distinct than for times when Λ_{uux} is low. This suggests that these vortical structures give a major contribution to the large macroscale. The streamwise vorticity is quite weak. The maximum v and w velocities in figure 8(*b*) are 0.045 whereas the streamwise velocity perturbation reaches a level of 0.18.

To study the evolution of the streak structures a local Gaussian filter was applied to the u-fluctuation fields for a number of consecutive times. The filter is given by

$$\tilde{u}(x,z) = \frac{\pi}{l_x l_z} \int\int u(\xi,\zeta) \exp\left(-\pi^2 \left[\frac{|x-\xi|^2}{l_x^2} + \frac{|z-\zeta|^2}{l_z^2}\right]\right) \mathrm{d}\xi \mathrm{d}\zeta. \tag{3.1}$$

The streamwise filter length l_x was chosen as one integral length (Λ_{uux}) and the spanwise filter length l_z corresponds to roughly the length at which the spanwise correlation ($R_{uu}(\Delta z)$) has its first zero-crossing. The filter length was defined on the spectral side of the filter as where the filter function is larger than 1/e. On the physical side the filter lengths become l_x/π and l_z/π. The first picture in figure 9 shows the entire midplane ($y = 0$) filtered u-field which clearly illustrates the organized structure of the large-scale velocity field. The following pictures show the evolution of a small part of the domain. Note that the mean propagation velocity of the structures is zero at the centreline. One can observe an instability-like break-up of the structures resulting in small-scale turbulence that in the filtered fields shows up as diffuse regions. A subsequent regeneration of the streaks can also be observed. This process is quite similar to the break-up regeneration cycle observed by Hamilton, Kim & Waleffe (1995) in a simulation of geometrically highly constrained Couette flow turbulence.

The two-point correlation for the different velocity components at $y = 0$ is shown in figure 10(*a,b*) as function of streamwise and spanwise separation, respectively. Results from the experiments of BTAA are included for comparison and show good agreement with the present data. The larger scales seen in the u-field in figure 7 are also reflected in the character of the correlation curves in figure 10. The streamwise integral scale Λ_{uux} is here 6.1 (see figure 6), which is almost eight times larger than in channel flow (see KMM).

The streamwise velocity correlation has a minimum at a spanwise separation of $\Delta z \approx 2$ (see figure 10*b*), which is consistent with the fact that the large structures essentially fill the entire gap between the plates and are close to circular in cross section (see figure 8*a,b*). Since they fill the whole channel in the wall-normal direction they do not contribute to the spanwise velocity at the centreline. This can be seen in the w-field in figure 7 which shows no sign of the large structures.

If the large structures had a preferred non-zero angle (with equal probability of plus and minus sign) with respect to the x-axis this would show up in a two-dimensional correlation surface $R_{uu}(\Delta x, \Delta z)$. However, figure 11 clearly shows that the largest correlation occurs for $\Delta z = 0$, indicating that the large structures are preferably aligned with the streamwise direction. This is also in agreement with the experimentally determined space–time correlation results recently obtained by Tillmark (1995).

In the u-field in figure 12 which is a grey-scale picture of the streamwise velocity in an (x,z)-plane at $y = 0.9$, or in wall coordinates $y^+ \approx 5$, we can observe the typical

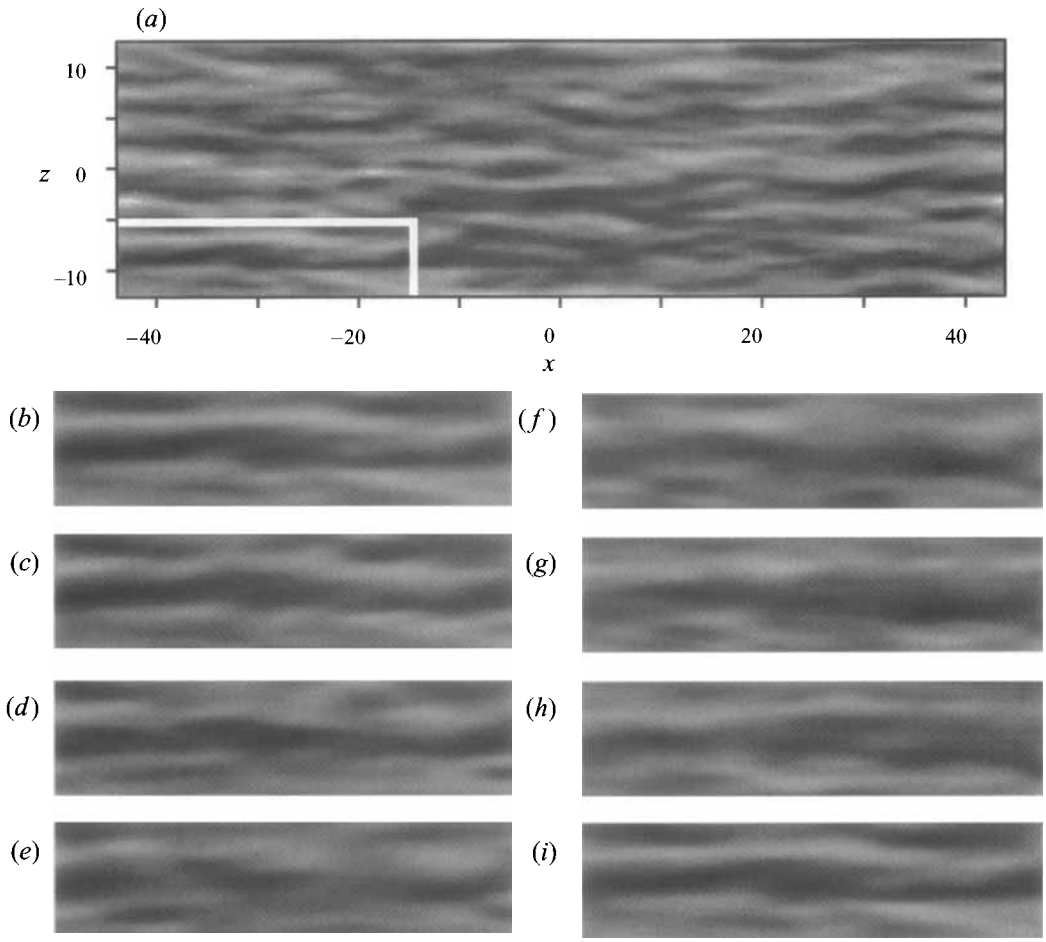

FIGURE 9. The filtered streamwise velocity for a series of consecutive times, at the midplane ($y = 0$). The velocity range is -0.3 to 0.3: (*a*) the whole (x,z)-plane, and (*b*–*g*) the lower left corner of the field (as marked in *a*), for different times. (*a*,*b*) $T = 1397.5$, (*c*) $T = 1402.2$, (*d*) $T = 1407.5$, (*e*) $T = 1413.4$, (*f*) $T = 1418.7$, (*g*) $T = 1424.0$, (*h*) $T = 1429.1$, and (*i*) $T = 1434.9$

wall streaks which here are more narrow than the elongated structures in the outer region. The wall normal velocity has a spatially very intermittent character, and associated high flatness at this position, which is roughly at the edge of the viscous sub-layer. The fluctuations in v are, of course, strongly damped by the wall at this position. We can observe signs of the wall streaks to some extent also in the spanwise velocity.

The correlations near the wall (figure 13) are here lower than at the centre of the channel. This is in contrast to channel flow, in which the lowest correlations occur at the centre. The positions of curves for v and w are opposite to those at $y = 0$. The minimum of the correlation for the streamwise velocity here occurs at a spanwise separation of $\Delta z \approx 1.3$, corresponding to $\Delta z^+ \approx 68$. This is some what larger than the corresponding value in channel flow. The wall streak spacing in channel flow (and other flows) is about 100 wall units, which should give a correlation minimum at $\Delta z^+ \approx 50$. The lack of scale separation associated with the low Reynolds number shows an influence of the large-scale outer structures even at this near-wall position.

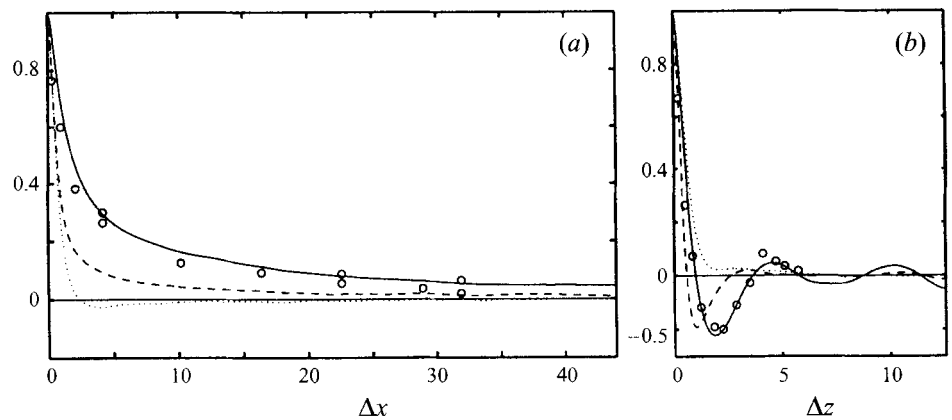

FIGURE 10. The two-point correlation, $R_{u_iu_i}$, for the streamwise (—), wall-normal (– –) and spanwise (· · ·) velocity at $y = 0$: (*a*) for streamwise separation, (*b*) for spanwise separation. Symbols (○) are from measurements by BTAA.

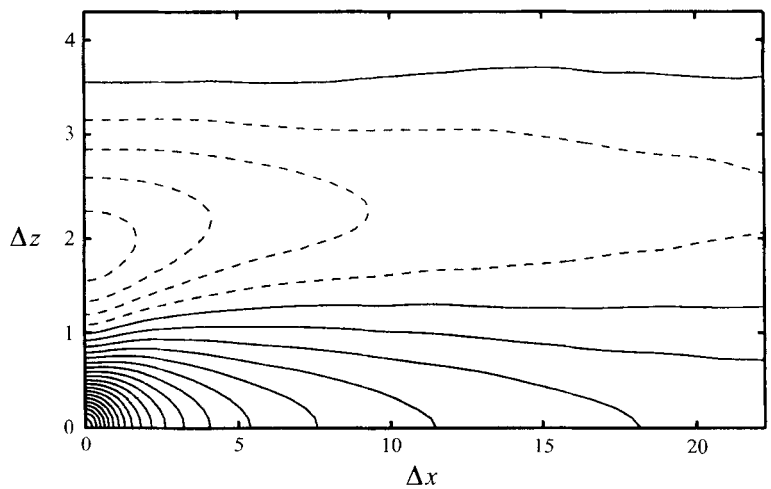

FIGURE 11. The two-point velocity correlation for the streamwise velocity as a function of streamwise and spanwise separation, $R_{uu}(\Delta x, \Delta z)$, at the midplane ($y = 0$). The positive contours denote $R_{uu} \geqslant 0$, and the dashed contours denote $R_{uu} < 0$. The contour increment is 0.05.

This causes the minimum to appear for a larger value than 50. In channel flow (see KMM) the u and w have correlation minima at the same spanwise separation $\Delta z^+ \approx 50$. Here the w velocity, which is less influenced by the largest outer structures, has a correlation minimum at $\Delta z^+ \approx 50$. It was also found that the correlations, as shown in figure 13, are essentially independent of wall distance in the viscous sub-layer.

3.1. *Statistical averages*

The statistical values presented here have, if not otherwise stated, been time averaged over 620 time units, and also averaged in space in the two homogeneous directions (x and z). The mean velocity profile non-dimensionalized by the friction velocity u_τ is shown in figure 14(*a*). Note the characteristic S-shape of the profile and the non-zero mean shear at the centreline, leading to non-zero turbulence production there. The

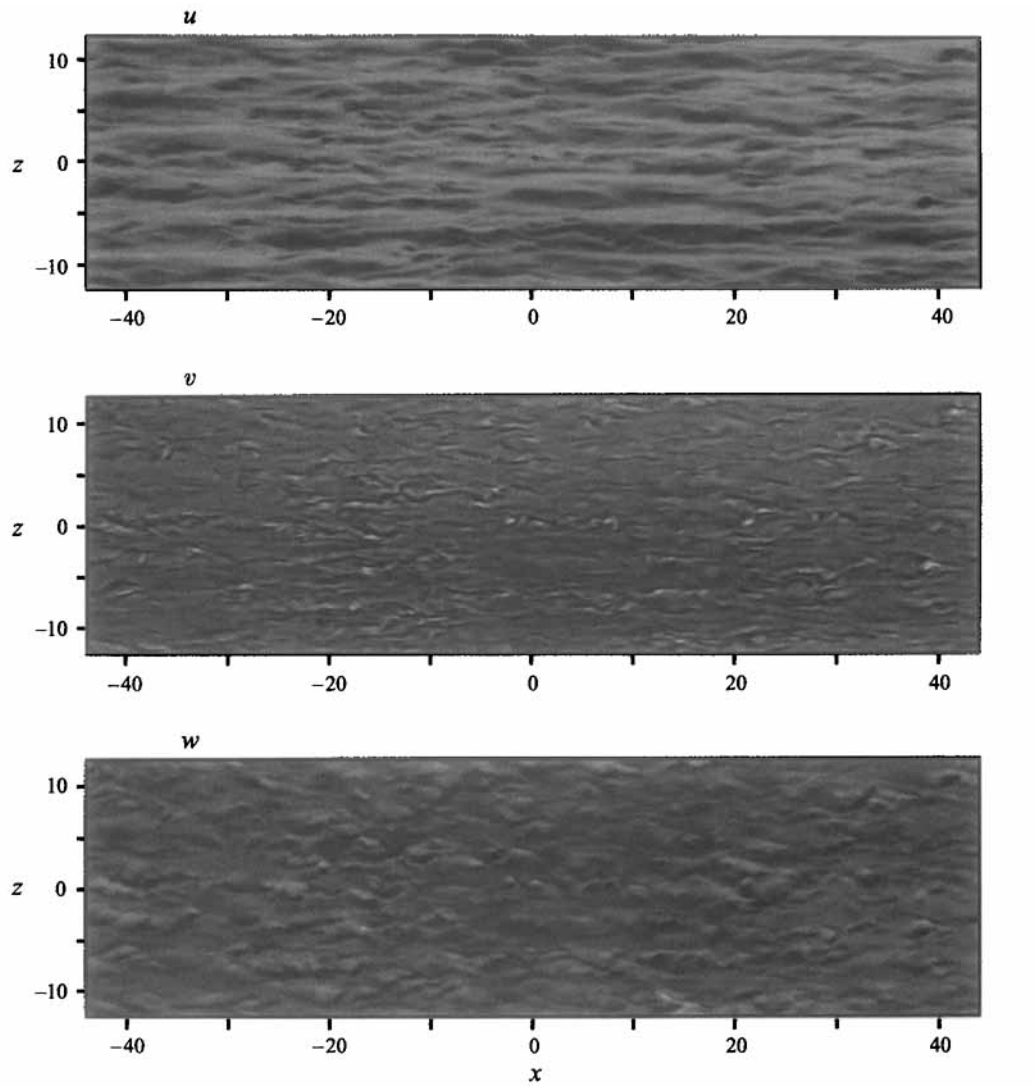

FIGURE 12. Instantaneous velocity fields at $T = 2020$ in an (x, z)-plane at $y = 0.9$. Streamwise velocity range 0.2 to 1.0; wall-normal velocity range −0.06 to 0.06; spanwise velocity range −0.3 to 0.3.

mean shear at the centreline $\mathrm{d}U/\mathrm{d}y|_{CL}$ is 0.18, or in wall units $\mathrm{d}U^+/\mathrm{d}y^+ = 0.05$. This means that the mean shear at the centreline is 1/20 of the mean shear at the wall. Tillmark (1995) compiled all existing experimental data for the shear at the centreline, which showed a practically constant, possibly very slowly decreasing value close to 0.2 for Reynolds numbers ranging from 750 to 19000.

The mean velocity in inner scales is presented in figure 14(*b*) in the classical semi-log plot. Note that the grid points closest to the wall are located at $y^+ = 0.09$. The dotted line in figure 14(*b*) represents the log-law with an additive constant of 4.6. Data from the experiments ($Re \approx 1300$) of BTAA are included for comparison. We note that the extent of the log-layer is very small due to the low Reynolds number. The y^+-value at the centreline is here only 52.0, which can be compared with the channel flow

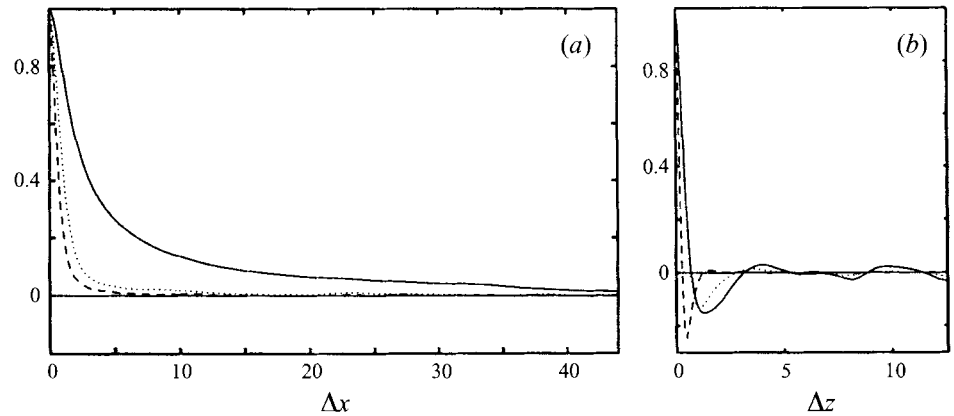

FIGURE 13. The two-point correlation, $R_{u_iu_i}$, for the streamwise (—), wall-normal (– –) and spanwise (· · ·) velocity at $y^+ \approx 5$: (*a*) for streamwise separation, (*b*) for spanwise separation.

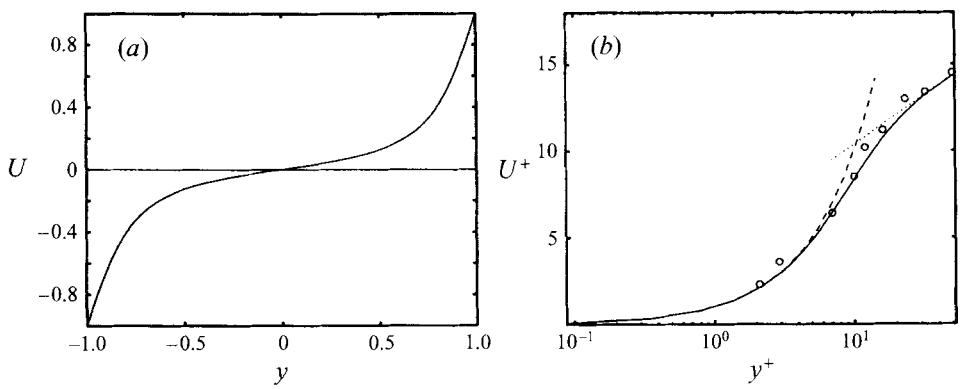

FIGURE 14. The mean velocity profile (*a*) in outer, and (*b*) in inner variables; ○ are from the experiments by BTAA. Dashed curve: $U^+ = y^+$. Dotted line: $U^+ = (1/0.4)\ln y^+ + 4.6$.

simulation of KMM where $y^+_{CL} \approx 180$. Despite the low y^+-value at the centreline in the present case the Reynolds number is about twice the transitional one.

Turbulence intensities for the three velocity components are shown in figure 15, where several things can be noted (y is the distance from the centre of the channel whereas y^+ is measured from one of the walls). The max u_{rms}/u_τ is 2.76 which compares well with other wall-bounded shear flows. The streamwise turbulence intensity at the centreline is as high as 2.06, mainly due to the non-zero turbulence production there. The low Reynolds number may also be of some influence, since the y^+-value at the centreline is lower so that the intensity should be compared with the corresponding value at the same y^+-value for a higher Reynolds number. This also means that the turbulence is considerably more anisotropic in the central part than, for example, in channel flow. The Reynolds number variation of u_{rms}/u_τ at the centreline appears to be quite weak and most experimental data fall close to 2.0. There is a close agreement with the experimental data of BTAA in the near-wall region.

There is considerable discrepancy in turbulence intensity near the centreline, which possibly could be ascribed to Reynolds number effects. A closer scrutiny of various investigations does not really support this hypothesis. Instead the results including

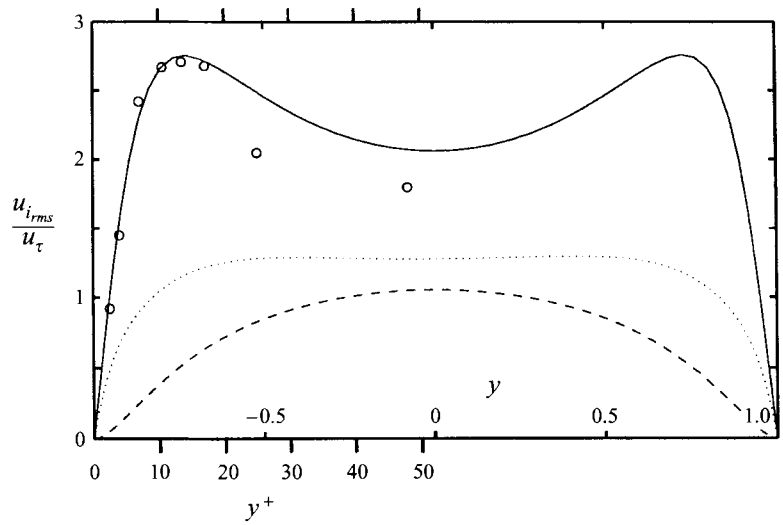

FIGURE 15. Root-mean-square velocity fluctuations normalized with the friction velocity: u_{rms}/u_τ (—), v_{rms}/u_τ (– –), w_{rms}/u_τ (···); ○ are experimental data from BTAA.

Reynolds number	Author	$u^+_{rms\|CL}$
1260	BTAA	1.60
1375	Tillmark (1995)	1.95
2300	Tillmark (1995)	1.95
2675	Tillmark (1995)	2.05
9500	El Telbany & Reynolds (1982)	1.74
1352	Aydin & Leutheusser (1991)	2.02
2381	Aydin & Leutheusser (1991)	1.96

TABLE 2. u^+_{rms} at the centreline as obtained in various investigations.

other experiments by Tillmark (1995) seem to indicate a value close to 2.0 irrespective of Reynolds number (see table 2). The w_{rms}-profile is almost constant in the central region. The same behaviour is observed by BTAA, Kristofferson *et al.* (1993) and Lee & Kim (1991), whereas in channel flow w_{rms} has a distinct minimum at the centre of the channel. The wall normal velocity in our simulation is monotonically increasing towards a maximum at the centreline. At higher Reynolds number a flatter curve would be expected in the central region.

The statistical errors in the turbulence intensity profiles are estimated in the same way as for the integral length scale. The estimated error obtained in this way is less than 1% of the maximum value.

The distribution of the Reynolds stress in plane Couette flow in figure 16 is seen to be symmetric in contrast to, for example, channel flow. For plane Couette flow one may readily integrate the streamwise momentum equation to obtain

$$\frac{dU^+}{dy^+} - \frac{\overline{uv}}{u_\tau^2} = 1. \tag{3.2}$$

Hence, the sum of the viscous and turbulent stress is constant throughout the channel. This also means that the deviation of $-\overline{uv}/u_\tau^2$ from unity at the centreline is equal

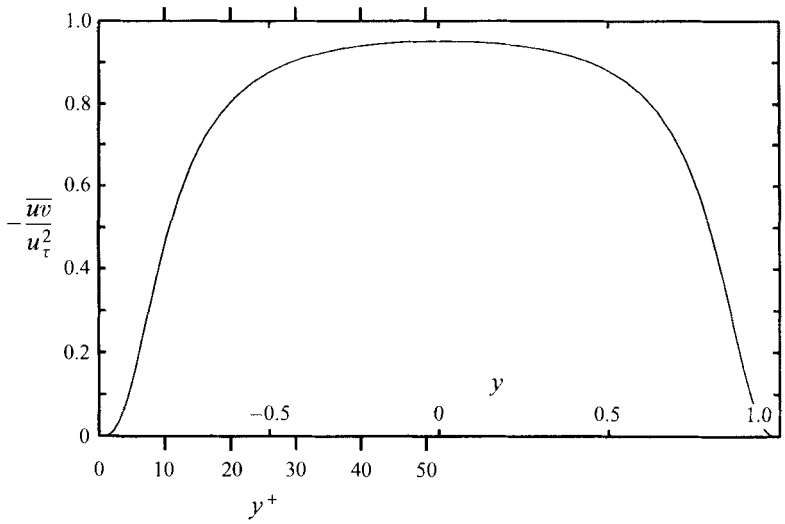

FIGURE 16. Distribution of the normalized Reynolds shear stress.

to the previously mentioned value of 0.05 for $\mathrm{d}U^+/\mathrm{d}y^+|_{CL}$. Here, the maximum Reynolds stress will occur at the centreline independent of Reynolds number. Hence, the general character of the curve in figure 16 is not a low Reynolds number effect.

If we expand the instantaneous velocities in power series about the wall values we see that the leading term in the Reynolds stress, $-\overline{uv}$, is of third order in y^+ close to the wall:

$$-\frac{\overline{uv}}{u_\tau^2} = ay^{+3} + \cdots. \tag{3.3}$$

Our simulation shows that $a = 1.2 \times 10^{-3}$. This is almost twice the value of 0.7×10^{-3} reported by Mansour, Kim & Moin (1988) for their investigation of channel flow. It is also higher than in the simulation of flow in a square duct by Gavrilakis (1992) where a value of about 0.8×10^{-3} was found.

The limiting value of the relative streamwise turbulence intensity, u_{rms}/U, or equivalently $(\omega_z^+)_{rms}$ has been the subject of much debate in the literature. Alfredsson *et al.* (1988) compiled and analysed previously reported experimental results and carried out a set of measurements in several different flow facilities. They concluded that earlier measurements with flush-mounted hot films in wind tunnels suffered from frequency-dependent heat loss to the hot-film-substrate, thus resulting in differences between the static and dynamic response characteristics. This effect results in a far too low value for hot films in air if a static calibration is used. Alfredsson *et al.* (1988) concluded from measurements in oil and water, and from measurements in air with a 'hot-wire on the wall', that the correct value of $(\omega_z^+)_{rms}$ should be close to 0.40. KMM obtained a value of 0.36 in their channel flow simulation, whereas a simulation at a higher Reynolds number yielded 0.40 (see Antonia & Kim 1994).

Gavrilakis (1992) simulated a square duct flow and reported a value of 0.36 at the duct wall bisector for $(\omega_z^+)_{rms}$. Here $(\omega_z^+)_{rms}$ approaches 0.41 at the wall.

It is noteworthy (see figure 17) that the intensities of the vorticity fluctuations in the central part are considerably higher here than in channel flow (by roughly three times).

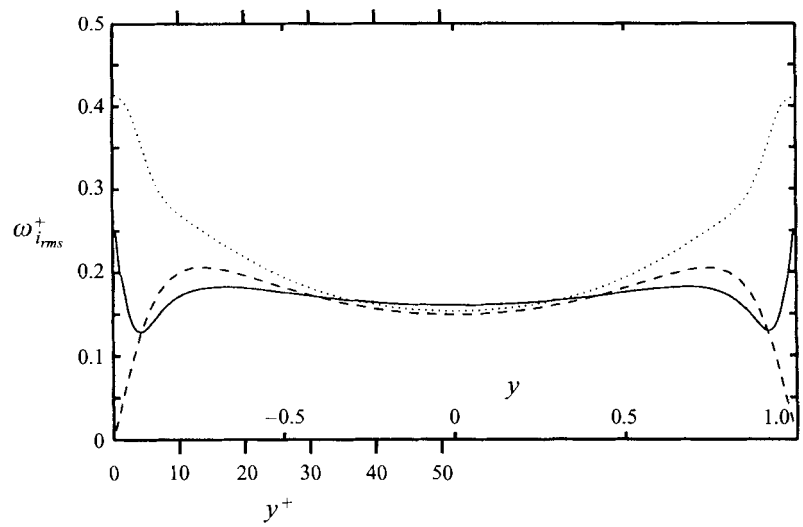

FIGURE 17. Root-mean-square vorticity fluctuations normalized by the mean shear: $\omega_{x_{rms}}\nu/u_\tau^2$ (—), $\omega_{y_{rms}}\nu/u_\tau^2$ (– –), $\omega_{z_{rms}}\nu/u_\tau^2$ (···).

The general character of the vorticity intensity curves is quite similar to that in channel flow (see KMM). Even the minimum in $(\omega_x^+)_{rms}$ occurs at the same y^+-position (approximately 5). KMM interpreted this as being related to the wall-normal extent of the wall streaks.

The skewness and flatness factors are shown in figure 18(*a,b*) and compared with results (for u) from the BTAA experiments. The Gaussian flatness value of 3 is included for comparison in figure 18(*b*). The almost perfect antisymmetry of the skewness curves shows that the statistical sample is adequate. Note that the zero crossing of S_u occurs where u_{rms} is a maximum and F_u is a minimum. This feature has also been found in a number of other flows.

The very high values of the flatness factor close to the wall, in particular for v, show the highly intermittent character of the flow in this region. This behaviour seems to be universal for all wall-bounded shear flows.

The turbulent kinetic energy budget can be written as (with $K = \frac{1}{2}\overline{u_i u_i}$)

$$\frac{\mathrm{D}K}{\mathrm{D}t} = \mathscr{P} - \epsilon - D \tag{3.4}$$

where, for parallel flow with variation in the y-direction only, the production $\mathscr{P}$, dissipation ϵ and the diffusion D are defined in non-dimensional form (scaled by U_w^3/h) as

$$\mathscr{P} = -\overline{u_1 u_2}\frac{\mathrm{d}U}{\mathrm{d}y},$$

$$\epsilon = \frac{1}{Re}\overline{\frac{\partial u_i}{\partial x_j}\frac{\partial u_i}{\partial x_j}},$$

$$D = \frac{\mathrm{d}}{\mathrm{d}y}\left[\frac{1}{2}\overline{u_i u_i u_2} + \overline{pu_2} - \frac{1}{Re}\frac{\mathrm{d}K}{\mathrm{d}y}\right].$$

For parallel flows each side of (3.4) is zero if we average over large enough times. We have explicitly calculated the production and the dissipation terms, and determined

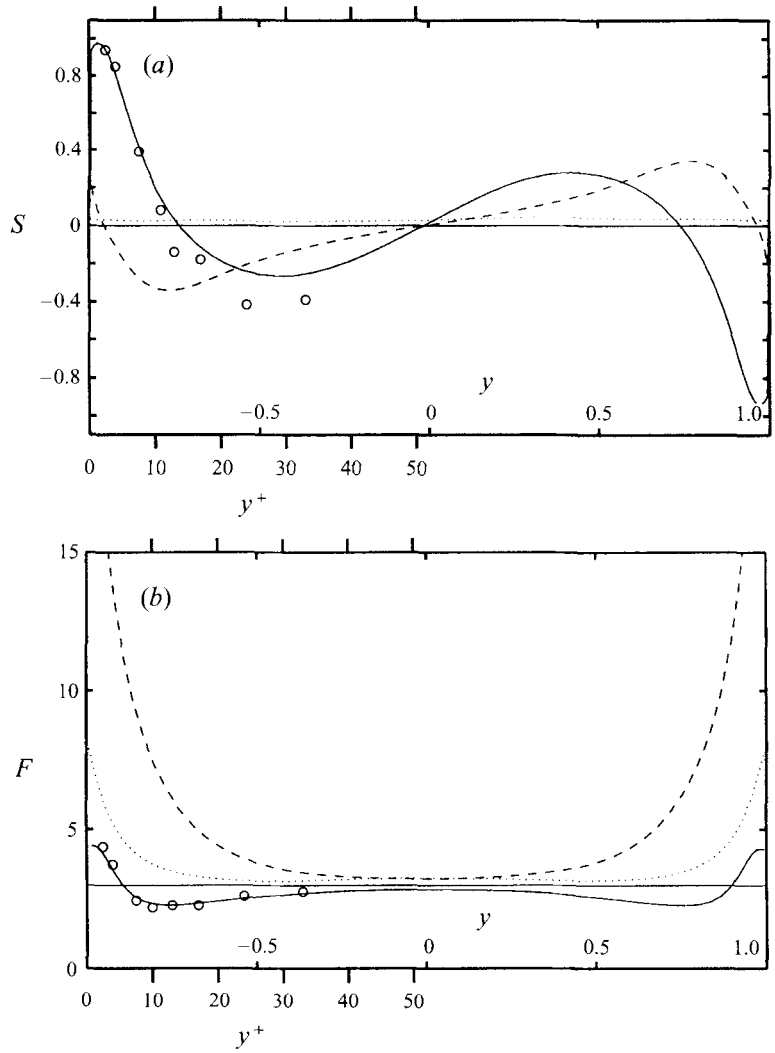

FIGURE 18. Skewness (*a*) and flatness (*b*) factors: u (—), v (– –), w (···); ○ are experimental data from BTAA.

the diffusion from the balance equation (3.4). To verify that this procedure yields a correct value of D, $\mathrm{D}K/\mathrm{D}t$ was determined and found to be less than 3×10^{-4} in the statistical sample used here. The diffusion term acts only as a spatial redistribution term, so the integral

$$\int_0^1 D \, \mathrm{d}y$$

should be zero. In the present statistical sample it is quite close to zero (−0.002). The value of the integral may be compared with that of the production, which was found to be 0.11. Altogether, this indicates that the above procedure is justified.

The distributions of $\mathscr{P}$, ϵ, and D between the two plates are shown in figure 19 and compared with the corresponding distribution from the channel flow simulation at $Re_\tau = h^+ = 180$ (Mansour *et al.* 1988). The general character of the curves is similar

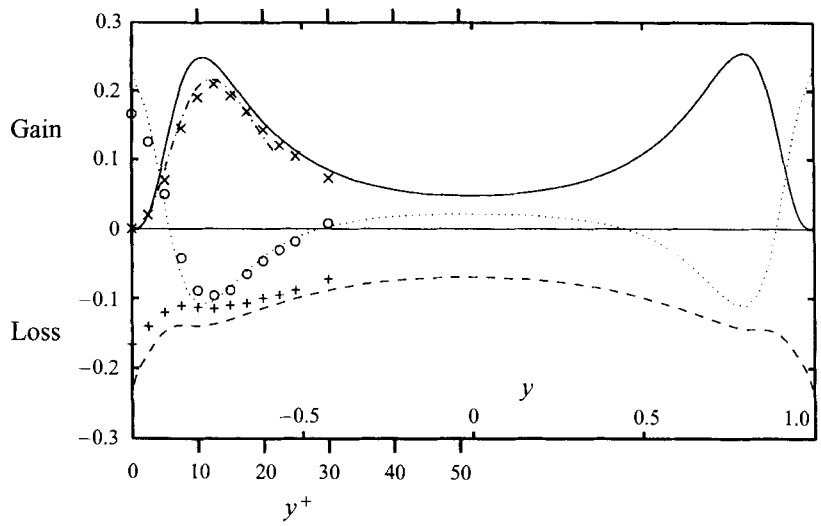

FIGURE 19. The turbulent kinetic energy budget: $\mathscr{P}$ production (—), ϵ dissipation (– –), and D diffusion (· · ·). Symbols are from Mansour *et al.* (1988) plotted as function of y^+: — · —, is the theoretically estimated production in a channel with a near-wall mean velocity approximated by $U^+ = (1/c)\tanh cy^+$.

		Channel	
Quantity	Couette	$h^+ = 180$	$h^+ = 400$
u^+_{rms}/y^+	0.41	0.36	0.40
v^+_{rms}/y^{+2}	1.3×10^{-2}	0.85×10^{-2}	1.1×10^{-2}
w^+_{rms}/y^+	0.26	0.19	0.25
$-\overline{uv}^+/y^{+3}$	1.2×10^{-3}	0.7×10^{-3}	1.0×10^{-3}
ϵ^+	0.23	0.16	0.22
ω^+_y/y^+	3.2×10^{-2}	2.7×10^{-2}	2.9×10^{-2}

TABLE 3. Limiting values for $y^+ \to 0$ (note that $\omega^+_z = u^+_{rms}/y^+$ and $\omega^+_x = w^+_{rms}/y^+$ here). Channel flow data from simulations (see Antonia & Kim 1994).

for the two cases. The distributions for the diffusion term are practically identical for the two cases.

Kim & Gibson (1989) hypothesized that there exists a large region of counter-gradient diffusion of turbulent energy from the centre of the channel towards the walls, caused by excess energy production at the centre of the channel. In fact, as our data show, there is no excess energy at the centre, instead the dissipation is larger than the production and the diffusion is towards the centre from $y^+ \approx 14$ and up, and towards the wall for smaller y^+-values. This can be seen more clearly if we model the diffusion by

$$D = \frac{\mathrm{d}}{\mathrm{d}y}\left[a\frac{\mathrm{d}k}{\mathrm{d}y}\right],$$

integrate both sides and divide by $\mathrm{d}k/\mathrm{d}y$. If a is less than zero we have counter gradient diffusion. Our data show no significant region with negative values of a and, hence, no counter-gradient diffusion.

For fully developed parallel shear flows in the channel flow geometry we can integrate the streamwise momentum equation once. For plane Couette flow we obtain (3.2). In the corresponding equation for fully developed channel flow a term $-y^+/h^+$ should be added to the right-hand side. By multiplying (3.2) by $\mathrm{d}U^+/\mathrm{d}y^+$, we obtain the following relation for the turbulence production in plane Couette flow:

$$\mathscr{P}^+ \equiv -\frac{\overline{uv}}{u_\tau^2}\frac{\mathrm{d}U^+}{\mathrm{d}y^+} = \frac{\mathrm{d}U^+}{\mathrm{d}y^+}\left(1 - \frac{\mathrm{d}U^+}{\mathrm{d}y^+}\right). \tag{3.5}$$

This means, for instance, that the turbulence production on the centreline is 0.05×0.95. This is verified in figure 19 where the terms in the energy budget are shown. From (3.5) it also directly follows that the maximum of $\mathscr{P}^+$ is 0.25 occurring at a position where $\mathrm{d}U^+/\mathrm{d}y^+ = 0.5$. This rather remarkable result for turbulent Couette flow is exact and holds irrespective of the value of the Reynolds number. This result is well reproduced in the present simulation results, and true also for channel flow and practically all wall-bounded shear flows to a high degree of accuracy for reasonably high Reynolds numbers.

For turbulent channel flow the expression (3.5) for the turbulence production would be modified by adding the term $-y^+/h^+$ within the parentheses. In the region where the production is large this additional term is quite small. The maximum of $\mathscr{P}^+$ approaches 0.25 for infinite Reynolds number, and we may estimate the deviation from this value by approximating the mean velocity profile with some analytical expression. It has been shown that the mean velocity profile from the wall up through the buffer region may be reasonably well approximated by

$$U^+ = \frac{1}{c}\tanh cy^+$$

with $c = 1/13.6$. This gives a maximum of $\mathscr{P}^+$ that occurs close to $y^+ = 12$. For the channel flow simulation described in Antonia & Kim (1994) the above expression gives $\mathscr{P}^+_{max}$-values of 0.217 for $h^+ = 180$ and 0.235 for $h^+ = 400$, which agree well with the data of Antonia & Kim (see also figure 19).

The above also means that the present Couette flow results in the near-wall region could be expected to resemble the high-Re ($h^+ = 400$) channel flow results more closely than the low-Re ($h^+ = 180$) case. This is evident from limiting values (as $y^+ \to 0$) of the various quantities given in table 3. For instance, we note that the previously discussed limiting value of u^+_{rms}/y^+ in the present simulation shows considerably closer agreement with the $h^+ = 400$ channel flow case, and is quite close to the value found from experimental studies in Alfredsson *et al.* (1988). An interesting aspect is that the limiting values for the present Couette flow simulation, hence, may be of interest for modelling purposes, where we may see these as values valid for high Reynolds number channel and boundary layer flows. The conclusion that the present near-wall results at $Re = 750$ should be valid also for higher Reynolds numbers is further substantiated by recent experimental results of Tillmark (1995). He measured u^+_{rms}/y^+ at $Re = 1260$ and 2300 and also found a limiting value in the viscous sub-layer of 0.41 for both these Reynolds numbers.

4. Effects of a weak system rotation

Simulations with various degrees of system rotation were carried out to study the sensitivity of the large-scale structures. The axis of rotation is chosen to be aligned with the spanwise direction and the sign is chosen to stabilize the flow. In contrast

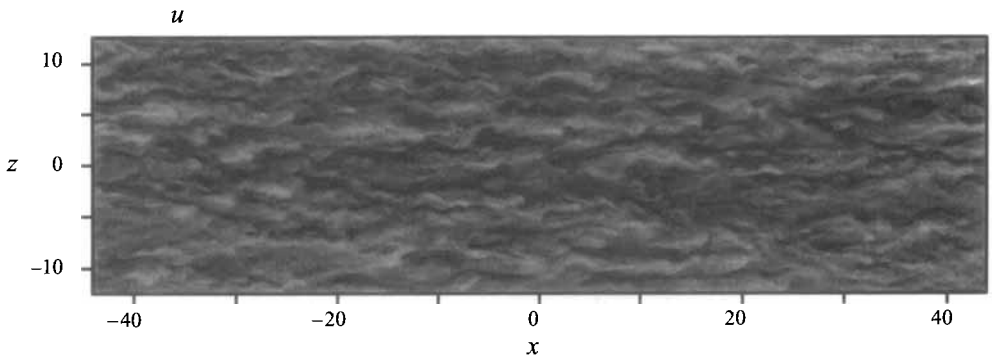

FIGURE 20. Instantaneous velocity fields in an (x, z)-plane at $y = 0$, $\Omega = -0.005$, streamwise velocity range -0.5 to 0.5.

to channel flow with stationary walls, both sides of the channel are here stabilized or destabilized if the sign of rotation is switched. The latter case has recently been studied by Bech (1995). Their results show enhanced turbulent fluctuations and distinct streamwise roll cells, for a destabilizing rotation.

The instability mechanism may qualitatively be understood by using a displaced-particle argument (see also Alfredsson & Persson 1989). The Coriolis acceleration of a fluid particle in a rotating system is defined as $\overline{a_c} = 2\overline{\Omega} \times \overline{U}$, where $\overline{\Omega}$ is the system rotation defined in figure 1, and $\overline{U}$ is the mean velocity. This acceleration will be directed normal to both the velocity vector and the rotation vector. In the present case the system rotation axis is aligned with the spanwise (z) axis, and the mean velocity is in the streamwise (x) direction. Hence, the body force associated with the Coriolis acceleration, which in non-dimensional form is written as $-2\overline{\Omega} \times \overline{U}$, will be aligned with the wall normal, and the sign will depend on the sign of the rotation. For a positive sign of the rotation the Coriolis force will increase monotonically from the lower ($y = -1$) to the upper wall ($y = +1$). Consequently there will be a monotonic decrease for $\Omega < 0$. We may here make the analogy with density-stratified situations. A monotonic decrease of the body force, corresponding to a decreasing density in the y-direction, gives a stable situation. Hence, here we should expect a stabilizing influence throughout the flow for $\Omega < 0$ and a destabilizing effect of a positive rotation.

In turbulent channel flow, one side of the channel will be stabilized and the other destabilized since $\mathrm{d}U/\mathrm{d}y$ is antisymmetric with respect to the centreline.

The dramatic effect on especially the large structures is evident in figure 20, where the applied system rotation is as weak as -0.005. Compared with the non-rotating field shown in figure 7 we clearly see that the extremely regular large-scale pattern there has disintegrated in figure 20. In the BTAA experiments where the half-channel width was 1 cm and the wall velocity was 0.13 m s^{-1}, the chosen non-dimensional rotation rate would correspond to one revolution in 100 s! The mean vorticity at the centreline (for $\Omega = 0$) is -0.18. The system rotation chosen here corresponds to an addition of -0.01 to this vorticity. This minor disturbance has a large dynamic effect and we see in figure 21 that the effect on the mean vorticity in the near-wall regions is about 50 times larger than the added vorticity, and almost one order of magnitude larger at the centreline. The effect is to reduce the difference in mean vorticity, i.e. to approach the laminar state, where $\overline{\omega_z} = -1$ throughout the channel. This tendency is further enhanced for the higher rotation rate ($\Omega = -0.015$) in figure 21. A further doubling of the rotation rate leads to relaminarization of the flow.

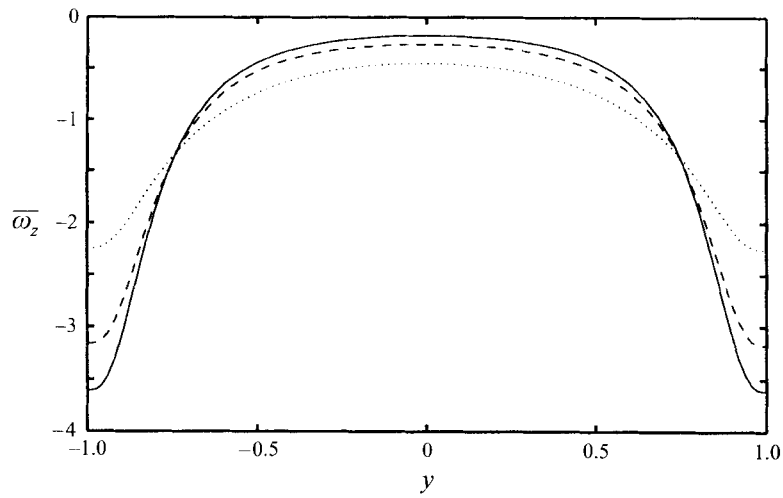

FIGURE 21. Mean spanwise vorticity $\overline{\omega_z}$ for different rotation rates: $\Omega = 0$ (—), $\Omega = -0.005$ (– –), and $\Omega = -0.015$ (· · ·).

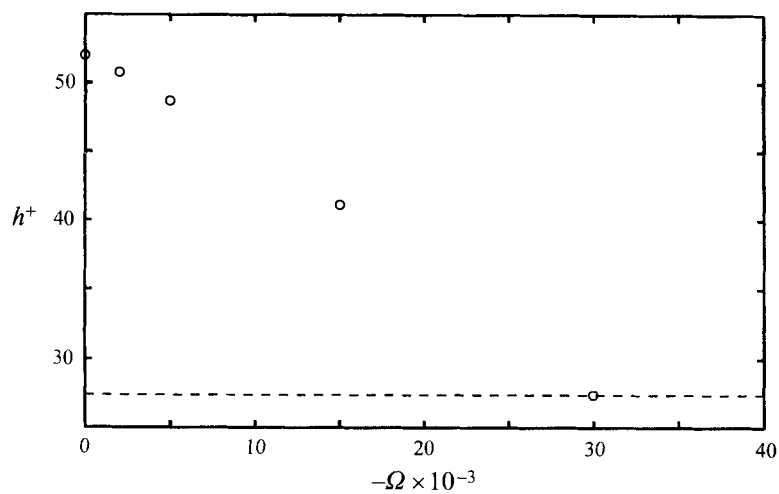

FIGURE 22. h^+ as a function of the rotation rate Ω: – –, laminar value.

The decrease in turbulent activity can be illustrated by the global measure h^+ which is also the friction-velocity Reynolds number of the flow. Figure 22 shows the monotonic decrease in h^+ as the rotation rate is successively increased. At $\Omega = -0.030$ the h^+ value is that of the laminar flow at this Reynolds number. Even at $\Omega = -0.015$ laminar regions start to appear in the flow.

In the computations the rotation rate was increased in steps to avoid large transients. For each rotation rate the simulation was carried out for long enough times for the transients to die out in the approach to steady state.

One may note that the change in h^+ at $\Omega = -0.005$ is quite small despite the dramatic change in the u-field appearance. This reflects the fact that only a small portion of the energy is contained in the very large structures. The excess energy associated with the elongated structures was estimated from spectra (see the discussion in connection with figure 2) to be roughly 10% of the total fluctuation energy.

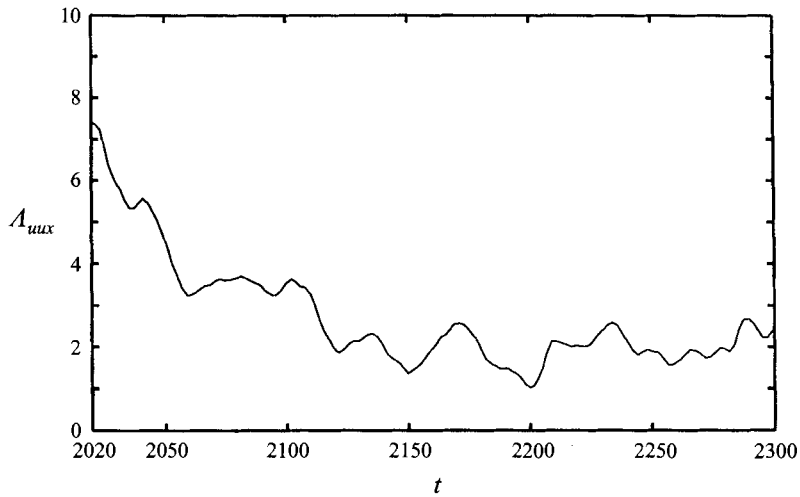

FIGURE 23. The integral length scale $\Lambda_{uux}(t)$ at $y = 0$ for a rotation rate Ω of -0.005. The rotation was applied at $T = 2020$.

The dramatic change in the flow field is illustrated in terms of velocity vectors and u-fluctuation velocity contours in the cross-stream (y, z)-plane in figure 8(*c*). In comparison with the non-rotating cases (figures 8*a*,*b*) the magnitude of the streamwise velocity fluctuations has decreased by roughly a factor of two and the break-up of the organized vortex structures is evident.

The break-up of large scales may be illustrated by the variation of Λ_{uux} with time. Figure 23 shows that we get a rapid decrease in the integral scale when the rotation is applied. At steady state Λ_{uux} approaches a value of about 2.0, i.e. only a third of that in the non-rotating case.

The correlation curves at the centreline for steady state with $\Omega = -0.005$ are compared with the corresponding non-rotating result in figure 24. The dramatic effect on the large scales mentioned above is clearly seen and the correlation drops to become insignificant at a streamwise separation of about 15 half-channel heights. Also the mean spacing between the structures decreases, from about $4h$ to about $2.6h$.

The corresponding correlation curves closer to the wall, $y^+ = 5$, are shown in figure 25. Here also the effect of the slow system rotation on the large structures is large, the correlation drops to zero at a streamwise separation of about $15h$, and the integral length scale Λ_{uux} drops from 5.6 to 3.0. Here the minimum for spanwise separation occurs for $\Delta z^+ \approx 50$, which corresponds to a mean spacing of the near-wall streaks of 100. Note that for the case with slow system rotation the integral length scale is higher close to the wall than in the centre of the channel, whereas in the case with no system rotation the reverse is true.

5. Concluding remarks

Direct numerical simulations of turbulent Couette flow were carried out at a Reynolds number of 750, based on half the velocity difference between the plates and the half-channel height. The simulations reveal the existence of very large-scale elongated structures qualitatively in accordance with earlier observations. Particular attention is, in this study, paid to the characteristics of these structures. To ensure reliable quantitative results the existence of these structures forces the computational

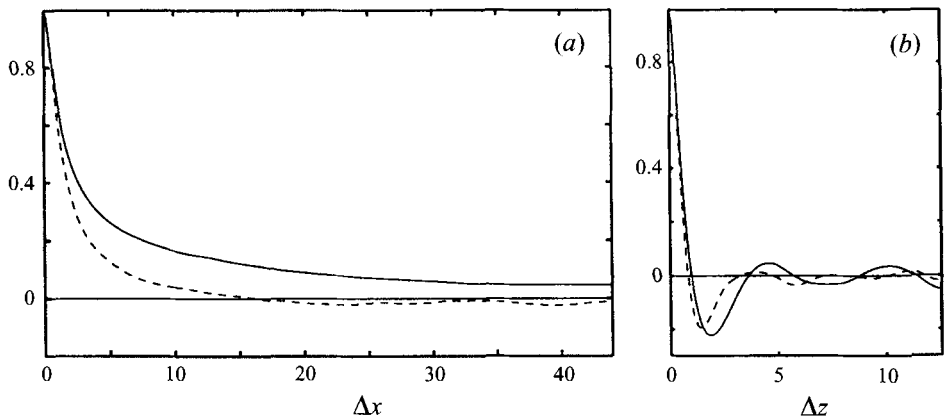

FIGURE 24. The two-point correlation for the streamwise velocity and different rotation rates at $y = 0$ and $\Omega = 0$ (—), $\Omega = -0.005$ (– –): (*a*) for streamwise separation, (*b*) for spanwise separation.

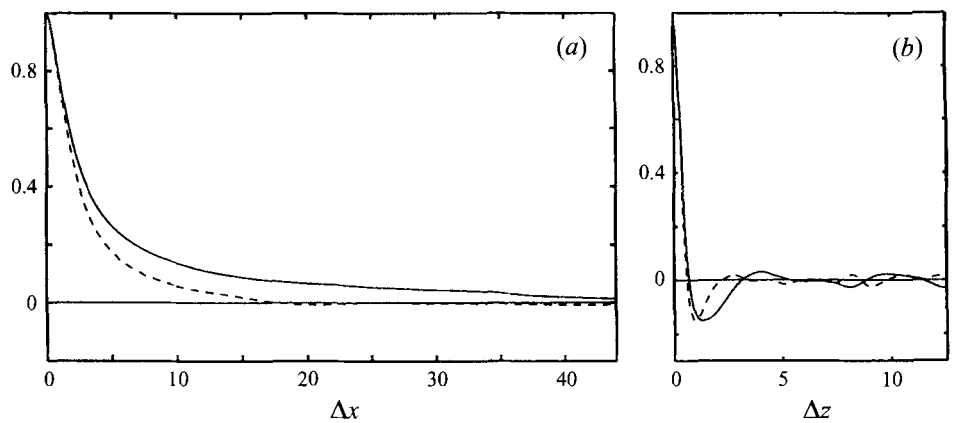

FIGURE 25. The two-point correlation for the streamwise velocity and different rotation rates at $y^+ = 5$, $\Omega = 0$ (—), $\Omega = -0.005$ (– –): (*a*) for streamwise separation, (*b*) for spanwise separation.

domain to be very large. The simulations reported here were carried out in a box approximately 42 times larger in area than that used for the channel flow simulations of KMM.

To confirm the convergence of the simulation results, simulations with several different box sizes were carried out. Comparisons with simulations in the smaller boxes suggests that the turbulent statistics for the largest box had converged to within 1% of the values valid for an infinitely large box.

In the channel flow simulation of KMM the streamwise integral scale, Λ_{uux}, on the centreline was found to be about 0.8. The present simulation shows that this scale is nearly eight times larger in plane Couette flow (at $Re = 750$). It is interesting to note that Gavrilakis (1992) showed with a numerical simulation that the integral scales in a square duct flow are significantly larger than in channel flow. Near a corner he found Λ_{uux}-values of about 1.6. This can be ascribed to the elongated structures formed by the secondary flow in that case.

A closer scrutiny of the large elongated structures in plane Couette flow is motivated by the fact that these form the major qualitative difference between this flow and canonical cases such as channel flow and zero-pressure-gradient boundary layer flow. The dynamics of the large structures and their role for the observed large integral scale was therefore further investigated by simulations of plane Couette flow with an imposed stabilizing system rotation (with the rotation axis in the spanwise direction). The effect on the large structures was shown to be dramatic even at very low rates of rotation. For an imposed rotation with a Rossby number of 200, which normally should signify negligible effects of rotation, the large elongated structures in the central region nearly vanished, resulting in a drop of the integral scale Λ_{uux} from about $6h$ to $2h$. The turbulence Reynolds number Re_τ, on the other hand, was observed to decrease by only a few percent, in accordance with the finding that the excess energy in the large structures is roughly only 10% of the total kinetic energy. This finding also indicates that the generation mechanism of the large structures is a very sensitive one.

The process of break-up–regeneration of the large streak structures was further studied by use of a spatially localized filter to remove the small scales. An instability-like break-up of the large structures could be observed similar to that found by Hamilton *et al.* (1995) in geometrically highly constrained Couette flow turbulence, similar in character to the evolution of near-wall structures observed by Johansson, Alfredsson & Kim (1991) in channel flow DNS data. The duration of the break-up–regeneration cycle was found to be of the order of 40–50 time units.

Extensive efforts were devoted to ensuring that accurate turbulence statistics could be obtained from the simulation. Good agreement was found with the experiments of Bech *et al.* (1995). The kinetic energy budget was studied in some detail. It was shown that the maximum of the turbulence production term $\mathcal{P}^+$ attains a value of 0.25, regardless of Reynolds number. This is also the value found in zero-pressure-gradient boundary layer flow and the asymptotic value for pressure-driven channel flow at infinite Reynolds numbers. This suggests a similarity between plane Couette flow and boundary layer flow as well as high-Re channel flow.

A comparison with previous channel flow simulations at two different Reynolds numbers (Antonia & Kim 1994) indeed showed that Couette flow data for limiting values of various quantities near the wall exhibit the closest similarity with the higher Reynolds number channel flow. Together with the fact that recent experimental findings also indicate that the limiting near-wall values are independent of Reynolds number in plane Couette flow, this means that the limiting values near the wall in the present Couette flow simulation may be close to those of high Reynolds number flow in channels and boundary layers, and may therefore be of interest for turbulence modelling purposes. An example might be the limiting value of the relative intensity of the streamwise wall-shear stress fluctuations, where experiments (Alfredsson *et al.* 1988) indicate a universal value in channel and boundary layer flows of about 0.40. The present value agrees well with the high-Re channel flow value of Antonia & Kim which also reconciles the discrepancy between the earlier low-Re channel flow simulation and the experimental findings.

REFERENCES

ALFREDSSON, P. H., JOHANSSON, A. V., HARITONIDIS, J. H. & ECKELMANN, H. 1988 The fluctuating wall-shear stress and the velocity field in the viscous sublayer. *Phys. Fluids* **31**, 1026–1033.

ALFREDSSON, P. H. & PERSSON, H. 1989 Instabilities in channel flow with system rotation. *J. Fluid Mech.* **202**, 543–557.

ANTONIA, R. A. & KIM, J. 1994 Low-Reynolds-number effects on near-wall turbulence. *J. Fluid Mech.* **276**, 61–80.

AYDIN, E. M. & LEUTHEUSSER, H. J. 1991 Plane-Couette flow between smooth and rough walls. *Exps. Fluids* **11**, 302–312.

BECH, K. H. 1995 Simulation of rotating and non-rotating turbulent plane Couette flow. Doctoral thesis, Department of Applied Mechanics, Thermodynamics and Fluid dynamics, Norwegian Institute of Technology, Trondheim.

BECH, K. H., TILLMARK, N., ALFREDSSON, P. H. & ANDERSSON, H. I. 1995 An investigation of turbulent Couette flow at low Reynolds numbers. *J. Fluid Mech.* **286**, 291–325 (referred to herein as BTAA).

EL TELBANY, M. M. M. & REYNOLDS, A. J. 1982 The structure of turbulent plane Couette flow. *Trans. ASME* I: *J. Fluids Engng* **104**, 367–372.

GAVRILAKIS, S. 1992 Numerical simulation of low-Reynolds-number turbulent flow through a straight square duct. *J. Fluid Mech.* **244**, 101–129.

HAMILTON, J. H., KIM, J. & WALEFFE, F. 1995 Regeneration of near-wall turbulence structures. *J. Fluid Mech.* **287** 317–348.

JOHANSSON, A. V., ALFREDSSON, P. H. & KIM, J. 1991 Evolution and dynamics of shear-layer structures in near-wall turbulence. *J. Fluid Mech.* **224** 579–599.

KIM, J., MOIN, P. & MOSER, R. 1987 Turbulence statistics in fully developed channel flow. *J. Fluid Mech.* **177**, 133–166 (referred to herein as KMM).

KIM, K. Y. & GIBSON, M. M. 1989 On modelling turbulent Couette flow. *Seventh Symp. on Turbulent Shear Flows: Open forum abstracts, Stanford University, California, Aug.* 21–23, pp. T8.1.1–T8.1.2.

KOMMINAHO, J., LUNDBLADH, A. & JOHANSSON, A. V. 1995 Determination of the transition Reynolds number in plane Couette flow through study of relaminarization. *Phys. Fluids* (submitted).

KRISTOFFERSON, R., BECH, K. H. & ANDERSSON H. I. 1993 Numerical study of turbulent plane Couette flow at low Reynolds number. *Appl. Sci. Res.* **51**, 337–343.

LEE, M. J. & KIM, J. 1991 The structure of turbulence in a simulated plane Couette flow. *Eighth Symp. on Turbulent Shear Flows Tech. University of Munich, Sept.* 9–11, pp. 5.3.1–5.3.6.

LUNDBLADH, A. & JOHANSSON, A. V. 1991 Direct simulation of turbulent spots in plane Couette flow. *J. Fluid Mech.* **229**, 499–516.

MANSOUR, N. N., KIM, J. & MOIN, P. 1988 Reynolds-stress and dissipation-rate budgets in a turbulent channel flow. *J. Fluid Mech.* **194**, 15–44.

PAPAVASSILIOU, D. V. & HANRATTY, T. J. 1996 Secondary flow and residual turbulence in plane Couette flow. In *Proc. Intl Conf. on Turbulent Heat Transfer San Diego, CA, March* 10–15. To appear.

REICHARDT, H. 1956 Über die Geschwindigkeitsverteilung in einer geradlinigen turbulenten Couetteströmung. *Z. Angew. Math. Mech.* **36**, 26–29.

REICHARDT, H. 1959 Gezetzmässigkeiten der geradlinigen turbulenten Couetteströmung. *Mitt. Max-Planck-Institut für Strömungsforschung* **22**.

ROBERTSON, J. M. & JOHNSON, H. F., 1970 Turbulence structures in plane Couette flow. *J. Engng Mech. Div. ASCE* **96**, 1171–1172.

TILLMARK, N. 1995 Experiments on transition and turbulence in plane Couette flow. Doctoral thesis, Department of Mechanics, Royal Institute of Technology, S-100 44 Stockholm.

TILLMARK, N. & ALFREDSSON, P. H. 1992 Experiments on transition in plane Couette flow. *J. Fluid Mech.* **235**, 89–102.